Functional and Structural Analysis of the Photosynthetic Apparatus of *Rhodobacter veldkampii*†

Francesca Gubellini,‡ Francesco Francia,§ Johan Busselez,‡ Giovanni Venturoli,§ and Daniel Lévy*,‡

Institut Curie, UMR-CNRS 168 and LRC-CEA 34V, 11 rue Pierre et Marie Curie, 75231 Paris Cedex 05, France, and Laboratory of Biochemistry and Biophysics, Department of Biology, University of Bologna, Via Irnerio 42, 40126 Bologna, Italy

Received May 19, 2006; Revised Manuscript Received July 6, 2006

ABSTRACT: In the widely studied purple bacterium *Rhodobacter sphaeroides*, a small transmembrane protein, named PufX, is required for photosynthetic growth and is involved in the supramolecular dimeric organization of the core complex. We performed a structural and functional analysis of the photosynthetic apparatus of *Rhodobacter veldkampii*, a related species which evolved independently. Time-resolved optical spectroscopy of *R. veldkampii* chromatophores showed that the reaction center shares with *R. sphaeroides* spectral and redox properties and interacts with a cytochrome bc_1 complex through a Q-cycle mechanism. Kinetic analysis of flash-induced cytochrome b_{561} reduction indicated a fast delivery of the reduced quinol produced by the reaction center to the cytochrome bc_1 complex. A core complex, along with two light-harvesting LH2 complexes significantly different in size, was purified and analyzed by sedimentation, size exclusion chromatography, mass spectroscopy, and electron microscopy. A PufX subunit identified by MALDI-TOF was found to be associated with the core complex. However, as shown by sedimentation and single-particle analysis by electron microscopy, the core complex is monomeric, suggesting that in *R. veldkampii*, PufX is involved in the photosynthetic growth but is unable to induce the dimerization of the core complex.

In purple photosynthetic bacteria, highly organized transmembrane pigment−protein complexes perform absorption of light and its conversion into chemical energy. Two light-harvesting (LH)[1] complexes, LH2 and LH1, ensure the collection of light. Then, the excitation energy is funneled toward the special pair (P) of bacteriochlorophylls in the reaction center (RC), followed by an electron transfer from P to ubiquinone (Q) acceptors Q_A and Q_B. After two photoreactions and proton captures, ubiquinol (QH_2) is formed at the Q_B site that dissociates from the RC into the membrane. The cytochrome bc_1 complex (cyt bc_1) utilizes QH_2 and oxidized cytochrome c_2 as the reductant and oxidant, respectively. The net result is a cyclic electron transfer that promotes the formation of a proton gradient across the membrane, which is utilized for ATP synthesis by F_1F_0-ATP synthase.

The description of the bacterial photosynthetic apparatus at the atomic level is nearly complete. Two RC structures (*1*−*3*), two LH2 structures (*4*, *5*), and the structure of the homologous cyt bc_1 complex from the respiratory chain (*6*) and recently from *Rhodobacter capsulatus* (*7*) are known. A crucial issue is the spatial organization between LH1 and the RC, forming the so-called core complex, in which the transformation of light energy into charge separation occurs.

In several photosynthetic organisms lacking LH2 (*Rhodospirillum rubrum* and *Blastochloris viridis*) or with atypical LH1-like LH2 (*Phaeospirillum molishianum*) as well as in *Rhodospirillum photometricum*, core complexes consist of a monomeric assembly of a central RC surrounded by an ellipse of α/β heterodimers. Different numbers of α/β LH1 heterodimers have been reported: 16 α/β possibly with a Ω subunit in *Rh. rubrum*, *B. viridis*, *Rh. photometricum*, and *P. molishianum* (*8*−*12*) and 15 α/β heterodimers plus a yet poorly characterized W peptide in *Rhodopseudomonas palustris* (*13*, *14*).

A notable exception is the dimeric organization of the core complex of *Rhodobacter sphaeroides* as shown by electron crystallography of tubular two-dimensional (2D) crystals present in LH2-deleted strains (*15*, *16*) and of 2D crystals of purified and reconstituted proteins (*17*, *18*). Furthermore, dimeric core complexes have also been imaged by atomic force microscopy (AFM) in native membranes of *Rhodobacter blasticus* (*19*). A number of 12−14 LH1 α/β heterodimers for *R. sphaeroides* have been proposed (*17*, *18*, *20*) and 13 for *R. blasticus* (*19*).

Several conditions of purification of the core complex of *R. sphaeroides* in different detergents have been reported (*17*, *18*, *21*−*23*). In all cases, dimeric core complexes have been isolated by sedimentation as the main population

† This study was supported by the European Community (IHP-RTN), the Human Frontier Science Program (to F.G.), the Ministere de la Recherche Française (to J.B.), the Curie Institut, the Centre National de la Recherche Scientifique, and the Commissariat à l'Energie Atomique. The financial support of MIUR of Italy is acknowledged by F.F. (PRIN 2005, "meccanismi molecolari e aspetti fisiopatologici dei sistemi bioenergetici di membrana"). F.F. was also supported by A. M. Contigliozzi and A. Contigliozzi.

* To whom correspondence should be addressed. E-mail: daniel.levy@curie.fr. Telephone: ++33-1-42346782. Fax: ++33-1-40510636.

‡ UMR-CNRS 168 and LRC-CEA 34V.

§ University of Bologna.

[1] Abbreviations: BChl, bacteriochlorophyll; DDM, *n*-dodecyl β-D-maltoside; DOTM, *n*-dodecyl β-D-thiomaltoside; OG, *n*-octyl β-D-glucopyranoside; EM, electron microscopy; LH, light-harvesting; RC, reaction center; cyt bc_1, cytochrome bc_1 complex.

10.1021/bi0610000 CCC: $33.50 © 2006 American Chemical Society
Published on Web 08/09/2006

coexisting with monomeric core complexes likely resulting from the dissociation of dimers. However, purified monomers reconstitute into dimers in lipid bilayers, suggesting a dimeric stable state in native membranes (*17*). Finally, spectroscopical analysis of the chromatophores and of the isolated purified dimeric and monomeric core complexes has highlighted the intracenter interactions, leading authors to propose that the dimeric core complex constitutes a privileged structure for antenna connectivity (*23*, *24*), a possibility that has been recently discussed on the basis of calculations of LH1 circular dichroism spectra (*25*).

Dimerization of the core complexes in *R. sphaeroides* has been unambiguously related to the presence in the core complex of a small polypeptide of ~80 amino acids, named PufX. This subunit is required for photosynthetic growth in *R. sphaeroides* under reducing conditions (*26*) and facilitates the diffusion of quinones from the Q_B site on the RC to the Q_o site on the cyt bc_1 complex (*21*). The precise localization of PufX is under debate, being within the LH1 assembly at the dimer junction (*17, 19*) or close to the inner α ring and the Qb site of the RC (*18*). Finally, PufX and/or the dimeric architecture is involved in the formation of long-range organization of core complexes (*15*, *27*−*29*).

So far, five *Rhodobacter* strains have been identified and classified into three subgroups on the basis of their 16S RNA sequence (*30*). A first subgroup is constituted by *R. sphaeroides* and *Rhodobacter azotoformans*, a second by *R. capsulatus* and *R. blasticus*, and a third, which diverged independently, by *Rhodobacter veldkampii*. A *pufX* gene has been found in all these *Rhodobacter* species.

Here we report the first characterization of the photosynthetic system of *R. veldkampii*. Time-resolved spectroscopy of chromatophores indicated that in *R. veldkampii* the redox midpoint potential of the primary donor P of the RC was similar to that measured in *R. sphaeroides* and that the cyclic electron transfer chain also operates according to a Q-cycle mechanism. Kinetic analysis of light-induced cytochrome b_{561} reduction under appropriate redox conditions showed that the quinone exchange between the RC Q_B site and the cyt bc_1 complex occurred at comparable rates. Three photosynthetic complexes, including the core complex and two types of LH2 complexes, were purified and analyzed by size exclusion chromatography, mass spectroscopy, and electron microscopy. The presence of a PufX subunit associated with the core complex was unambiguously identified by MALDI-TOF spectrometry. Strikingly, sedimentation experiments and single-particle analysis by electron microscopy reveal that the isolated RC−PufX−LH1 core complex of *R. veldkampii* is monomeric.

MATERIALS AND METHODS

Bacterial Strain, Growth Conditions, and Membrane Preparation. R. veldkampii strain DSM 11550 (from German Strain Collection of Microorganisms and Cell Culture, DSMZ, Braunschweig, Germany) was grown for 72 h (OD_{670} = 4 AU) under both photosynthetic and dark/semiaerobic conditions. Photosynthetic growth was carried out in Roux bottles containing MYS medium (*31*) at 28 °C with two 100 W spot lamps as a source of light. Dark/semiaerobic growth was performed at the same temperature, with shaking at 100 rpm in an Erlenmeyer flask filled to 50% of the total volume with MYS medium. *R. sphaeroides* strain ΔQ x/g deleted in the chromosomal *puf* operon (*32*) and complemented in trans with a low-copy number plasmid harboring a *puf* operon with or without the *pufX* gene was grown semiaerobically in Sistrom's minimal medium in the presence of kanamycin (25 μg/mL) and tetracycline (2 μg/mL) (*21*).

Chromatophores were prepared as previously described (*21*). Briefly, cells were disrupted with a French press and centrifuged to remove unbroken cells. Supernatant was ultracentrifuged in a Beckman type 45 Ti rotor for 90 min at 125000*g* (4 °C), resuspended in 50 mM glygly (pH 7.8), 1 mM EDTA, and 1 mM benzoamidine, and immediately frozen.

Optical Absorption Spectroscopy. Kinetic spectrophotometric measurements in chromatophores were performed in a N_2 atmosphere under controlled redox conditions (*33*). Samples were resuspended in 50 mM MOPS and 100 mM KCl (pH 7.00) containing *p*-benzoquinone, 1.2-naphthoquinone, and 1,4-naphthoquinone (10 μM each) as redox mediators. To avoid contributions due to BChl and carotenoid electrochromic absorption changes, membranes were uncoupled with valinomycin and nigericin (10 μM each).

A xenon flash lamp (EG&G FX201, discharging a 3 μF capacitor charged to 1.5 kV) was used for flash excitation, with a pulse duration at half-maximal intensity of 4 μs. The actinic flash was passed through a Wratten 88A Kodak filter, and the photomultiplier was protected with a Corning glass 4/96 filter. Absorbance changes were measured by a single-beam spectrophotometer of local design (*33*). A triggered shutter was used to gate the measuring beam limiting at 2 s the exposure of the sample to the measuring light before flash excitation. Data were acquired with a LeCroy 9410 digital oscilloscope interfaced with an Olivetti M240 personal computer.

The light minus dark spectra were recorded on a Jasco V-550 spectrophotometer; the sample was exposed to the light from the top with a flexible optic fiber. The exciting light, passed through a Kodak 88A glass filter, was provided by a quartz/tungsten halogen lamp (Oriel 6681) set at 100 W and the phototube protected with a Corning glass 4/96 filter.

Reduced minus oxidized spectra of chromatophores were obtained from oxidized spectra registered in the presence of 500 μM potassium ferricyanide and reduced spectra measured after addition of a few crystals of sodium dithionite. The final BChl concentration in the cuvette was 20 μM.

The midpoint redox potential of the primary electron donor P of the RC was estimated on a chromatophore suspension at 35 μM total BChl by varying the ambient redox potential by addition of potassium ferricyanide. The concentration of P still reduced at a given ambient redox potential was evaluated from the extent of P photo-oxidation induced by a train of eight actinic flashes fired at a frequency of 10 Hz. The concentration of P undergoing photo-oxidation was determined from the flash-induced absorption change at 542 nm using a differential extinction coefficient [$\Delta\epsilon_{542} = 10.3$ mM^{-1} cm^{-1} (*34*)]. The cyt bc_1 complex was inhibited by addition of 5 μM antimycin and 1 μM mixothyazol. Flash-induced kinetics of cytochrome b_{561} reduction were measured at 561−569 nm (*34*).

Isolation and Purification of Photosynthetic Complexes. Membranes were solubilized for 15 min at 4 °C in the dark

in 3.5% *n*-dodecyl β-D-thiomaltopyranoside (DOTM), and the photosynthetic complexes were separated on linear gradient of 11 to 33% (w/w) sucrose in 50 mM glygly (pH 7.6) and 0.1% DOTM (*17*). Alternatively, other procedures were used: solubilization in 3% *n*-octyl D-glucopyranoside (OG) and 0.5% sodium cholate and sedimentation in a sucrose gradient containing 0.6% OG and 0.2% sodium cholate (*21*, *22*) or solubilization in 3% β-dodecyl maltoside (DDM) and sedimentation in 0.03% DDM (*18*) or extraction of a small amount of total protein by 0.7% DDM and sedimentation in 0.1% DDM.

The three bands corresponding to two forms of LH2 complexes (LH2 and LH2′; see Results) and the core complex were extracted, dialyzed to remove the sucrose, and analyzed separately by size exclusion chromatography in 50 mM glygly (pH 7.6) and 0.1% DOTM. A size exclusion G200 column was previously calibrated with a high-molecular weight gel filtration kit from Amersham. Before FPLC analysis, the isolated core complexes were purified with a DEAE column at 400 mM NaCl (pH 7) to remove any trace of LH2 complexes. The concentration of the purified core complex (final Abs_{880}/Abs_{280} ratio of 1.9) was calculated using an extinction coefficient of 3.9 μM^{-1} cm^{-1} at 884 nm as in *R. sphaeroides* (F. Francia, unpublished results).

Peptide Mass Fingerprint. Purified core complexes were precipitated with 10 volumes of a cold acetone/methanol mixture (7:2, v/v) and centrifuged. The organic phase was discarded and the pellet dried at 40 °C for 40 min. The pellet was resuspended in 50 mM glygly (pH 7.8) and loaded on a 17% acrylamide SDS−PAGE gel stained with Coomassie G250. The putative band of PufX was cut out and subjected to an overnight in-gel trypsin treatment. Peptides were extracted from the gel by electroporation, analyzed by MALDI-MS, and sequenced by ES Q-Tof MS/MS analysis. Protein identification was achieved by mass fingerprint of peptides and comparison with the NCBI protein database (NCBI accession number BAD44691) using the Mascot algorithm.

Electron Microscopy. Aliquots (5 μL) of the core complex or LH2′ complex freshly purified by size exclusion chromatography were deposited on glow-discharged carbon-coated grids, negatively stained with 2% uranyl acetate, and sandwiched between two carbon films according to the method of ref *35*. This allowed better staining of small proteins than the conventional negatively stained procedure. Images were taken under low-dose conditions on a Philips CM120 microscope operating at 120 kV at 1.5 μm defocus, and a nominal magnification of 45000×, with a 1024 pixel × 1024 pixel Gatan ssCCD camera. The pixel size, calibrated using bacteriorhodopsin 2D crystals, was 3.9 ± 0.1 Å.

A total of 425 projections of the LH2′ complex (see the text) were analyzed by ImageJ after a Gaussian filter application. Particles with more than 90% circularity were selected.

A total of ∼2500 single projections of the core complex were manually windowed and centered. Self-organizing mapping (SOM) segmented by multivariate statistical analysis, kernel probability density estimator SOM (KerDenSOM) (*36*), and maximum likelihood multireference alignment (*37*) were used to identify six homogeneous groups of projection. The images belonging to those classes were aligned using a free reference algorithm (*38*) before average images were computed. The resolution of the average images was estimated to 24 Å using the FRC method. X-mipp (*39*) was used for image processing except for multivariate statistical analysis, which was performed with SPIDER (*40*).

RESULTS

Thermodynamic and Spectral Features of the Cyclic Electron Transfer Chain. In uncoupled *R. veldkampii* chromatophores, i.e., in the presence of 10 μM valinomycin and nigericin, light-induced absorbance changes measured between 500 and 600 nm, attributed to the oxidation of the primary electron donor P of the RC, were similar to those detected in *R. sphaeroides*. By monitoring at 542 nm the flash-induced absorption changes due to formation of P^+ as a function of the ambient redox poise (E_h), we obtained a titration curve characterized by a midpoint potential (E_m) of 470 ± 5 mV (data not shown). This E_m value for the P^+/P redox couple was close to values determined in the related photosynthetic bacterium *R. sphaeroides*, for which reported E_m values range from 440 to 495 mV (*41*, *42*).

Reduced minus oxidized spectra of chromatophores from *R. veldkampii* show a large absorption band peaking at 562 nm, characteristic of *b*-type hemes from the ubiquinol-cytochrome *c* oxidoreductase (cyt bc_1 complex) and a shoulder/peak at ∼552 nm typical of *c*-type cytochromes. As shown in Figure 1A, the spectral contribution of *b*-type cytochromes was more pronounced in the light-grown membranes of *R. veldkampii* than in membranes from semiaerobically grown cells. This suggests a higher *b*-type/*c*-type ratio in photosynthetic membranes or a larger loss of soluble *c*-type cytochromes during preparation of chromatophores from photosynthetically grown bacteria.

To confirm the presence of a cyt bc_1 complex involved in a cyclic electron transfer and operating in a Q-cycle, we tested the sensitivity of light-induced absorbance changes in the cytochrome *b* spectral region to inhibitors of the bc_1 complex. Chromatophores, poised at a redox potential of 400 mV and inhibited with 5 μM antimicin, were excited by four actinic flashes, and the flash-induced absorption changes were recorded as a function of the measuring wavelength. Then, 1 μM myxothiazole was added to the sample, and the measurements were repeated. Experimental traces recorded at 561 nm are shown in Figure 1B. The differences between the traces with antimycin and antimycin with myxothiazole were measured 300 ms after the last flash and plotted as a function of wavelength between 545 and 575 nm. The resulting spectrum (Figure 1C), which peaks at 561 nm, revealed that a cytochrome *b* heme (cyt b_{561}) was stably reduced following flash excitation in the presence of antimycin in a myxothiazole sensitive reaction.

Kinetics of Cytochrome b_{561} Reduction Induced by a Single-Turnover Flash under Oxidizing Redox Conditions. According to the Q-cycle mechanism (for a recent review, see ref *43*) in the oxidation of ubiquinol at the Q_o site of the bc_1 complex, the first electron released by QH_2 reduces in sequence the iron−sulfur center and the cytochrome c_1 (high-potential chain of the complex), while the second electron reduces sequentially hemes b_{566} and b_{561} (low-potential chain). When the high-potential chain of the complex is reduced in the dark before flash excitation, the oxidation of

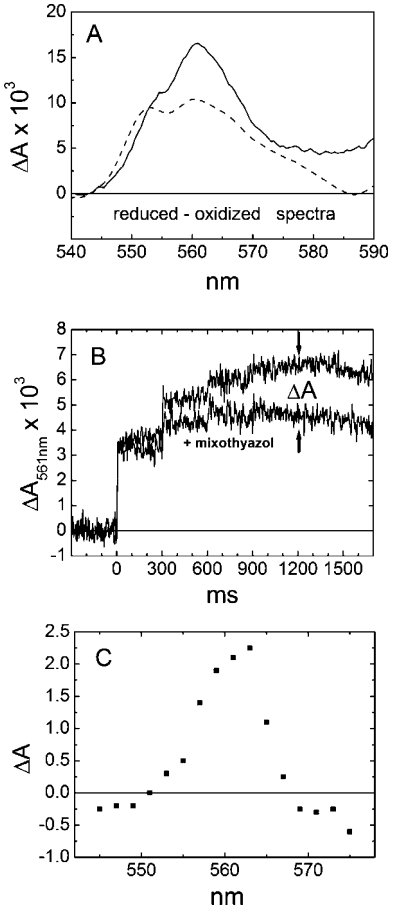

FIGURE 1: Sensitivity of *b*-type hemes to the bc_1 complex inhibitors. (A) Reduced minus oxidized spectra of *R. veldkampii* chromatophores (20 μM BChl) from photosynthetically (—) and semiaerobically (- - -) grown bacteria. Oxidized spectra recorded in the presence of 500 μM potassium ferricyanide and reduced spectra after addition of sodium dithionite. Spectra were averaged four times. The absorption band peaking at 562 nm is typical of *b*-type hemes from the bc_1 complex. The shoulder at 551 nm and the peak at 555 nm are attributed to *c*-type cytochromes. (B) Absorbance changes at 561 nm induced by trains of four actinic flashes 300 ms apart. The ambient redox potential was maintained at 400 mV by adding potassium ferro/ferricyanide. The top trace was in the presence of 5 μM antimycin and the bottom trace after addition of 1 μM myxothiazole. The arrows indicate the time (300 ms after the fourth flash) where the difference before and after the addition of myxothiazole has been evaluated. (C) Absorbance difference with and without myxothiazole (ΔA indicated in panel B) as a function of the detection wavelength.

QH_2 at the Q_o site requires therefore that soluble cytochrome c_2, oxidized by the flash-generated P^+, react with the bc_1 complex, draining an electron from the high-potential chain, i.e., oxidizing in sequence cyt c_1 and the Rieske Fe−S center. At low concentrations of soluble cyt c_2, this reaction can become rate-limiting in the turnover of the bc_1 complex and in principle contribute to the lag which is observed between the time of the flash and the onset of cyt b_{561} reduction at the full rate. At variance, when the ambient redox potential is sufficiently high (E_h > 350 mV), the iron−sulfur center is chemically oxidized and ready to accept the first electron delivered by QH_2. Moreover, under these oxidizing conditions, the only ubiquinol available to the Q_o site is the one produced by the photoactivity of the reaction center at the Q_B site. Therefore, in chromatophores redox poised at sufficiently high E_h values, the lag is uniquely related to the time needed for release of ubiquinol from the Q_B site and its diffusion to the Q_o site of cytochrome bc_1. A kinetic analysis of cyt b_{561} reduction under these conditions can therefore yield information about the quinone-mediated redox interaction between the RC and the bc_1 complex.

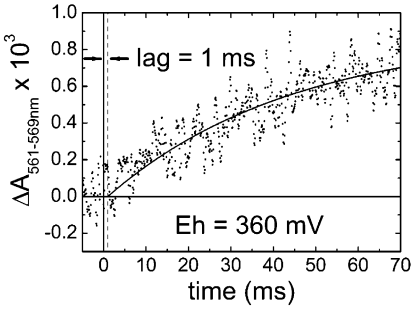

FIGURE 2: Reduction of heme b_{561} in a single-turnover flash. Chromatophores were resuspended at 30 μM BChl at an ambient redox potential maintained at 360 mV by the addition of 500 μM potassium ferrocyanide. The experimental trace (dotted mode) is the difference between the absorbance change recorded at 561 and 569 nm. For each wavelength, 25 signals have been averaged. The best fitting monoexponential function (—) has been used to estimate the delay time (lag) between the flash-induced stimulation of the RC (time zero, vertical solid line) and the beginning of the heme b_{561} reduction kinetics (vertical dotted line).

Chromatophores from *R. veldkampii* inhibited with antimycin were poised at an E_h of 360 mV, and the absorbance change induced by a single-flash stimulation was recorded at 561−569 nm (Figure 2). To determine the lag between the time of the flash (continuous vertical line in Figure 2) and the onset of the cyt b_{561} reduction (dashed vertical line), traces were fitted to an exponential function and the lag time before the onset of the first-order kinetics was varied stepwise from time zero (corresponding to the actinic flash). For each lag period, χ^2 was minimized by adjusting the amplitude and the half-time of the exponential kinetics and a plot of χ^2 values versus the lag was obtained (*44*). Following this procedure, a lag time of 0.5−1.5 ms has been estimated in *R. veldkampii* chromatophores. The range given for the lag period corresponds to a 1% increase of χ^2 around the best fitting value (*44*). To compare directly the kinetics of cyt b_{561} reduction in *R. veldkampii* and *R. sphaeroides*, the same measurements (under strongly oxidizing conditions) were repeated in chromatophores from the latter species, using both the wild-type (WT) and pufX-deleted (ΔX) strains. These measurements yielded a lag of 1−2 ms for the WT and 10−15 ms for the ΔX strain (data not shown). This indicates that in *R. veldkampii* and WT *R. sphaeroides* the rate of transfer of quinol produced by the RC to the Q_o site of the bc_1 complex is on the same time scale of 10^{-3} s.

Isolation of Photosynthetic Complexes. Photosynthetic complexes from photosynthetically and semiaerobically grown cells were purified by sedimentation on a sucrose density gradient after extraction using DOTM, a mild detergent that was shown to stabilize the dimeric core complex of *R. sphaeroides* (*17*). As shown in Figure 3A, three bands were separated in the sucrose gradient. The denser band exhibited a LH1−RC absorption spectra presenting typical peaks of carotenoids at 488, 456, and 432 nm, LH1 (Q_y at 884 nm and Q_x at 592 nm), and RC (BChl at 804 nm and BPheo at 760 nm). Strikingly, the two other bands in the gradient exhibited near-infrared peaks at 804

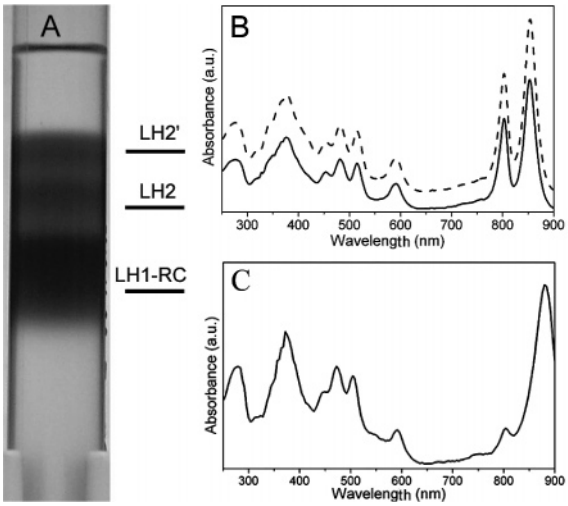

FIGURE 3: Purification of photosynthetic complexes from *R. veldkampii*. (A) Membrane complexes from photosynthetically grown *R. veldkampii* were solubilized and separated on a sucrose gradient in three distinct bands, LH2, LH2′, and LH1−RC. (B) Absorbance spectra of LH2 (—) and LH2′ (- - -) exhibit an identical absorption pattern characteristic of LH2 complexes with near-infrared peaks at 804 and 854 nm. (C) Absorbance spectra of the purified core complex.

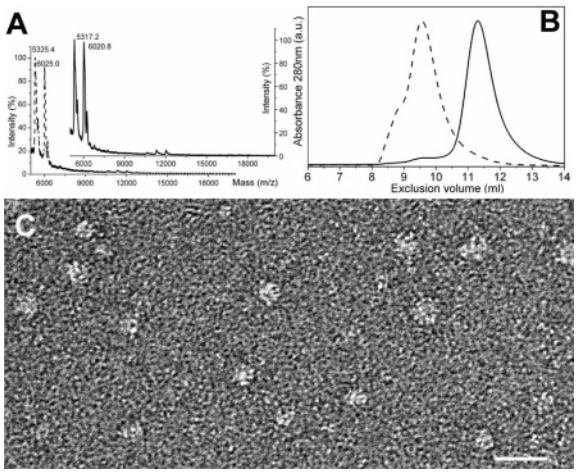

FIGURE 4: Characterization of LH2 complexes of *R. vedlkampii*. (A) MALDI-TOF spectra of purified LH2 (—) and LH2′ (- - -) with nearly identical molecular masses of the α and *β* subunits. (B) Size exclusion chromatography of LH2 (—) and the significantly larger LH2′ complex (- - -). (C) Electron micrograph of purified LH2′ showing a round-shaped particle 12 ± 1 nm in diameter. The bar is 25 nm.

and 854 nm characteristic of LH2 complexes (Figure 3B; see also Figure 5B) and were therefore ascribed to two forms of the peripheral antenna, LH2 (bottom band) and LH2′ (top band). LH2 and LH2′ were isolated from the DOTM sucrose gradient, dialyzed to remove the sucrose, and run separately in a second DOTM gradient. Again, LH2 and LH2′ sedimented as a unique band but at different buoyant densities, revealing stable complexes.

Solubilization and purification with DDM or a mixture of OG and cholate instead of DOTM or lowering the total amount of extracted proteins also led to three well-separated bands (see Materials and Methods). Thus, we propose that the three isolated complexes were present in the native membrane and were not resulting from any dissociation and reassociation of complexes during the isolation procedure.

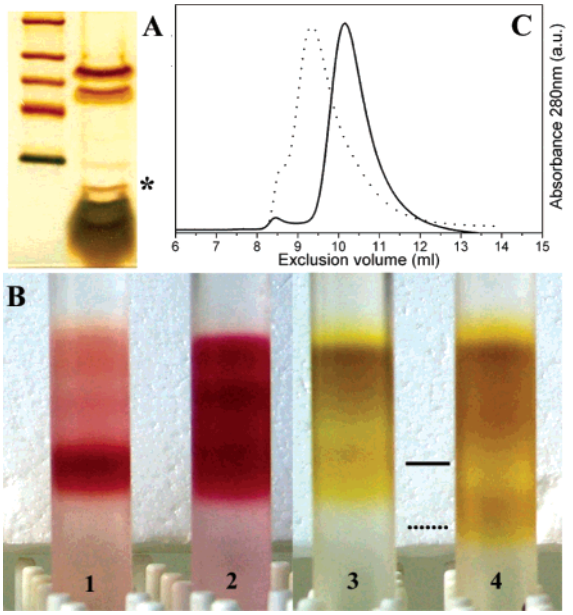

FIGURE 5: Oligomeric state of the core complex of *R. veldkampii*. (A) SDS−PAGE of the purified core complex of *R. veldkampii*. The asterisk denotes the PufX band. (B) Size exclusion chromatography of the core complexes of *R. veldkampii* (—) and the dimeric core complex of WT *R. sphaeroides* (dotted line). (C) Sucrose gradients of solubilized membranes from *R. veldkampii* photosynthetically (1) or semiaerobically (2) grown. Sucrose gradients of solubilized membranes from the *R. sphaeroides* ΔX strain (3) with monomeric core complexes (—) and from WT (4) with dimeric core complexes (···).

Analysis of LH2 Complexes. LH2 and LH2′ were further analyzed by MALDI-TOF (Figure 4A), revealing a nearly identical polypeptide composition. Two main peaks were found for LH2 (5317.2 and 6020.8 Da) and LH2′ (5325.4 and 6025.0 Da) and assigned to *β* and α subunits respectively, according to *R. sphaeroides* (*β* at 5457 Da and α at 6809 Da). Others peaks originated from homo- and heterodimeric association of α and *β* subunits.

Size exclusion chromatography of LH2 (Figure 4B) revealed a single peak eluting at 11.4 mL, close to LH2 from *R. sphaeroides* (11.3 mL). LH2′ corresponded to a significantly larger complex eluting as a broader peak with a maximum at 9.5 mL. The fraction at 9.5 mL was analyzed by electron microscopy (Figure 4C), revealing particles 12 ± 1 nm in diameter ($n = 425$). This is significantly larger than the 7 nm nonameric LH2 from *R. sphaeroides* (*45*) or *Rhodopseudomonas acidophila* (*4*) or the decameric LH2 observed by AFM of the native membrane of *Rh. photometricum* (*46*). However, this complex might be similar to the large LH2 complexes that are ∼10 nm in diameter present as a minor population in *Rh. photometricum* (*46*).

RC−LH1 Complex. The core complex isolated from the sucrose gradient was further purified by DEAE chromatography to remove any trace of LH2 followed by size exclusion chromatography. The purified core complex was analyzed by gel electrophoresis, revealing the RC subunits between 29 and 36 kDa, LH1 polypeptides α and *β* at 5−7 kDa, and an additional band at ∼9 kDa (asterisk), the expected molecular mass of PufX (Figure 5A). Subunits M and H, overlapping in the gel in Figure 5B, were separated at a lower acrylamide concentration (10%).

MALDI-TOF analysis confirmed this assignment with peaks at 5.4 kDa for the *β* subunit, 6.7 kDa for α LH1

Table 1: Sequence Analysis of PufX from *R. veldkampii*[a]

observed molecular mass (Da)	peptide sequence
1232.59	AEKHYLDGATK
1195.53	VGMATMGAAAMGK
2293.06	EAPYPNTIFQVNDIDGTVDGK
2713.26	EAPYPNTIFQVNDIDGTVDGKYTR

N-ter 1-MAEKHYLDGATKVGMATMGAAAMGKGMGI-28
29-TAVVFFGTVFFVVALAFIGQFLPDRSR-56
57-EAPYPNTIFQVNDIDGTVDGKYTR FAN-83 C-ter

[a] The putative PufX band extracted from a SDS−PAGE gel (asterisk in Figure 5B) was trypsinized, and the fragments that were obtained, underlined in the sequence of PufX, were analyzed by MALDI-TOF. Four peptides were identified as being derived from the pufX gene of *R. veldkampii* by comparison with the NCBI database.

subunits, and 34.9, 31.4, and 28.1 kDa for RC H, L, and M subunits, respectively (data not shown). The 9 kDa band was extracted from the gel, trypsinized, and further analyzed by MALDI-TOF. By using the Mascot software, the identified masses were matched to peptide sequences (Table 1) and were finally ascribed to the PufX protein of *R. veldkampii* by comparison with the NCBI database. An ES Q-Tof MS/MS analysis performed on these peptides for amino acid sequence information revealed fragments at N- and C-termini of the PufX sequence. The formylmethionine at the N-terminus was absent as previously found in PufX proteins isolated from *R. capsulatus* and *R. sphaeroides* (*43*). It is therefore possible that it is usually not maintained in the protein after translation. The last three amino acids at the C-terminus where a trypsin restriction site is found upstream were missing, likely because they were too small to be detected in the mixture of fragments. It is thus concluded that the PufX subunit was present in the core complex of *R. veldkampii*.

Oligomeric State of the R. veldkampii Core Complex. Four sucrose gradients were run in parallel to compare the density in a DOTM sucrose gradient of the photosynthetic complexes extracted from *R. veldkampii* grown photosynthetically (tube 1), semiaerobically (tube 2), or from *R. sphaeroides* ΔX and WT strains (tubes 3 and 4, respectively) (Figure 5B). The core complex of *R. veldkampii* sedimented as a unique band positioned at the same density of the monomeric complex in the ΔX strain of *R. sphaeroides* (lower band in tube 3, solid line). No core complex at the dimeric level (indicated by the dimeric core of *R. sphaeroides*, tube 4 and the dotted line) was detected whatever the conditions of solubilization and separation in OG and cholate and in DDM (see Materials and Methods). It is important to stress that even solubilization with a minimal amount of DDM gave the same monomeric band. Furthermore, the isolated core complex analyzed by gel size exclusion (Figure 5C, solid line) exhibited a single peak at 10.2 mL corresponding to a complex significantly smaller than the dimeric RC−LH1 complex from *R. sphaeroides* (Figure 5C, dashed line).

Single-Particle Analysis. Single-particles analysis was performed upon a set of negative stain EM images of the purified core complex. Because of the small size of the core complex for the single-particle analysis, ∼300 kDa, the contrast was enhanced by using the negative staining and sandwich approach that provides better staining than the conventional negative staining. A representative EM field

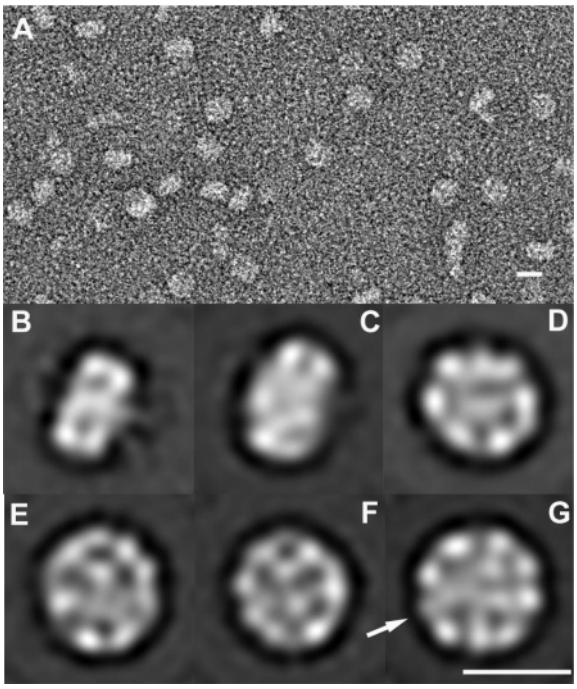

FIGURE 6: Single-particle 2D analysis of the core complex of *R. veldkampii*. (A) Electron micrograph of the negatively stained purified core complex of *R. veldkampii*. (B−G) Average projections of the six classes found after classification, averaging, and filtering at 24 Å resolution. Panel B corresponds to the side view and panel G the top view, and panels C−F correspond to tilted views of the core complex. The arrow in panel G depicts a lower density in the LH1 assembly revealing an absence or a tilted peptide.

image is depicted in Figure 6A showing top views, a tilted view, and side views of the purified complex; 1850 particles were extracted, classified, and averaged in six major populations representing 19 (B), 18 (C), 21 (D), 11 (E), 14 (F), and 17% (G) of the particles. The average was filtered at the resolution given by the FRC method (∼24 Å). Panels B and G of Figure 6 depicted averages of side views and top views of the core complex, respectively, while other averages corresponded to tilted views of the core complex. As seen in the top average view (Figure 6G), the core complex consisted of the LH1 ring encircling a central nonresolved density of the RC. The LH1 ring has an outer diameter and an inner diameter of ∼115 and ∼75 Å, respectively, values consistent with the data from other strains such as *Rh. rubrum* [outer of 115 Å and inner of 65 Å (*41*, *42*)], *Rhd. palustris* [elliptic LH1 complex, outer ring of 110 Å × 95 Å and inner ring of 78 Å (*13*, *14*)], and *Rhodopseudomonas viridis* [elliptic LH1 complex with an outer diameter of 104 Å × 98 Å (*11*)]. Density was roughly homogeneous along the LH1 ring. However, a lower density was present in the LH1 ring in the average and in the raw data, revealing an absence of peptide or a tilted peptide in this region (arrow in Figure 6G).

DISCUSSION

We have found that the photosynthetic apparatus of *R. veldkampii* is similar to that of the better characterized *R. sphaeroides and R. capsulatus* species in several aspects. (i) The midpoint potential of the P^+/P redox couple of the RC is 470 mV (*41*, *42*). (ii) In the presence of antimycin A, a flash-induced reduction of cyt b_{561} is observed on the

millisecond time scale, inhibited by myxothiazole (Figure 1C). (iii) The reduced quinol molecule produced by the RC under strongly oxidizing conditions is promptly available at the Q_o site of the bc_1 complex, as shown by the short lag of 1 ms, as in WT *R. sphaeroides*, observed in the cyt b_{561} reduction kinetics (Figure 2). By comparison, the lag period in the absence of PufX (ΔX *R. sphaeroides*) under identical redox conditions was increased to 10−15 ms. Such an increase in the lag period in the absence of PufX had been previously reported under less oxidizing conditions (E_h = 200 mV) (*44*). Comayras and colleagues (*23*, *24*) examined the reduction kinetics of cyt b_{561} in a similar experiment and found that in the absence of pufX the lag increased, although to a lesser extent (∼2 ms). To account for this discrepancy, the authors suggest tentatively that the longer lag could be due to a limitation in cytochrome c_2. These measurements performed at an E_h of 360 mV, i.e., under conditions in which the high-potential chain of the complex is already oxidized before the flash, show that this was not the case. As a whole, these results showed that cyt b_{561} reduction kinetics measured under oxidizing conditions in chromatophores from *R. veldkampii* and wild-type *R. sphaeroides* were similar.

In *R. veldkampii*, the requirement of PufX for anaerobic, photosynthetic growth has not been proven by deletion of the pufX gene as it was for *R. sphaeroides* (*47*) and *R. capsulatus* (*48*). However, our analysis of cyt b_{561} reduction kinetics showed that the quinol−quinine exchange at the Q_B site of the RC occurred in *R. veldkampii* membranes as fast as in wt *R. sphaeroides* chromatophores, suggesting that also in *R. veldkampii* the PufX protein facilitates the quinone-mediated interaction between the RC and the cyt bc_1 complex.

The RC−LH1 core complex of *R. veldkampii* contains a PufX protein unambiguously identified by MALDI-TOF (Table 1). However, only a monomeric form of the PufX−RC−LH1 core complex was biochemically isolated (Figure 5B) and confirmed by electron microscopy (Figure 6), although the different experimental conditions reported for the purification of the dimeric core complex in *R. sphaeroides* have been performed (*17*, *18*, *21*−*23*). Furthermore, several 2D crystallization trials of the core complex, including those leading to the formation of 2D crystals of the core complex of *R. sphaeroides* (*17*, *18*), have been performed. This led to large vesicles containing proteins that are closely packed without any appearance of the typical crystalline arrays constituted by dimeric complexes. It is worth noting that the purified monomeric core complex of *R. sphaeroides* resulting from the dissociation of the dimeric core complex in detergent dimerized in the lipid membrane upon reconstitution (*17*). Although the core complex of *R. veldkampii* could require specific conditions of 2D crystallization, we proposed that these results are consistent with a monomeric organization or with a much less stable dimeric organization of the core complex of *R. veldkampii* than in *R. sphaeroides* and *R. blasticus*, in the native membrane.

R. veldkampii has diverged separately from two other *Rhodobacter* subgroups constituted by *R. sphaeroides* and *R. blasticus* and *R. capulatus*, for which a dimeric core complex has been found (*15*, *17*, *19*) or proposed (*49*, *50*). A sequence comparison has led authors to propose that the PufX protein of *R. sphaeroides* and *R. capsulatus* derived from the N-terminus of the tetraheme cytochrome *c*, the protein encoded by the *pufC* gene (*51*). The *pufX* gene in the *Rhodobacter* genus is located in the operon at the same position as the *pufC* gene of *Roseobacter denitrificans* and in all the members of the *Rhodovulum* genus (*30*). Furthermore, a phylogenetic tree based on the 16S rRNA revealed that *Rhodobacter* and *Rhodovulum* genera diverged from a common ancestor and that in an earlier step *Roseobacter* was separated from them (*30*). It is thus possible that an "immature" form of the PufX protein present in *R. veldkampii*, unable to determine dimerization (or a stable dimer) of the core complex, also derived from the N-terminal part of the reaction center cytochrome *c* subunit. The evidence that in *R. sphaeroides* (*22*) and in *R. capsulatus* (*50*) the transmembrane region of the PufX protein is sufficient to allow a photosynthetic phenotype despite a loss of dimer stability supports this hypothesis. The PufX subunit of *R. sphaeroides*, *R. blasticus*, and *R. capsulatus* could have acquired in a subsequent step the ability to dimerize.

The structural motif of PufX that is involved in the dimerization of the core complex is not yet known. However, it has been found that N-terminal deletion of PufX in *R. sphaeroides* reduced the level of core complex dimerization, suggesting a role for amino acids 7−19 in the interaction between two PufX proteins (*22*). Alignment of the PufX N-terminus from *R. sphaeroides* (amino acids 9−16) and *R. capsulatus* (amino acids 9−16) reveals two conserved oppositely charged amino acids in the DxxNxxxK sequence that might be involved in the stabilization of the two monomers of the core complex. The corresponding DxxxK sequence in *R. veldkampii* might be too short for such interaction (*30*).

However, it has been demonstrated that the dimeric form of the core complexes in *R. sphaeroides* constituted a privileged structure for antenna connectivity (*23*). In view of the prompt reduction of cyt b_{561} observed in *R. veldkampii* chromatophores, our results revealed that a stable RC−LH1 dimer is not strictly required for an efficient release of quinol from the core complex. Hence, the functional role of the dimeric form of the RC−PufX−LH1 core complex, as suggested by the work of Comayras et al. (*23*, *24*) (however, see also ref *25*), could be related to optimization of light harvesting rather than facilitation of the quinol−quinone exchange between the RC and the cyt bc_1 complex.

ACKNOWLEDGMENT

We thank Dr. J. L. Rigaud for initiating the structural analysis of the photosynthetic complexes and for providing the environment that has made this work possible. We are grateful to Dr. S. Marco for his constant help during the different steps of the single-particle analysis, Dr. W. Faigle from the mass spectroscopy platform of the Curie Institut, and to Dr. K. V. P. Nagashima for his advice on the optimal growth of *R. veldkampii*.

REFERENCES

1. Deisenhofer, J., Epp, O., Miki, K., Huber, R., and Michel, H. (1984) X-ray structure analysis of a membrane protein complex. Electron density map at 3 Å resolution and a model of the chromophores of the photosynthetic reaction center from *Rhodopseudomonas viridis*, *J. Mol. Biol. 180*, 385−98.
2. Allen, J. P., Feher, G., Yeates, T. O., Komiya, H., and Rees, D. C. (1987) Structure of the reaction center from *Rhodobacter sphaeroides* R-26: The cofactors, *Proc. Natl. Acad. Sci. U.S.A. 84*, 5730−4.

3. Katona, G., Andreasson, U., Landau, E. M., Andreasson, L. E., and Neutze, R. (2003) Lipidic cubic phase crystal structure of the photosynthetic reaction centre from *Rhodobacter sphaeroides* at 2.35 Å resolution, *J. Mol. Biol. 331*, 681−92.
4. Papiz, M. Z., Hawthornthwaite, A. M., Cogdell, R. J., Woolley, K. J., Wightman, P. A., Ferguson, L. A., and Lindsay, J. G. (1989) Crystallization and characterization of two crystal forms of the B800−850 light-harvesting complex from *Rhodopseudomonas acidophila* strain 10050, *J. Mol. Biol. 209*, 833−5.
5. Koepke, J., Hu, X., Muenke, C., Schulten, K., and Michel, H. (1996) The crystal structure of the light-harvesting complex II (B800−850) from *Rhodospirillum molischianum*, *Structure 4*, 581−97.
6. Xia, D., Yu, C. A., Kim, H., Xia, J. Z., Kachurin, A. M., Zhang, L., Yu, L., and Deisenhofer, J. (1997) Crystal structure of the cytochrome bc_1 complex from bovine heart mitochondria, *Science 277*, 60−6.
7. Berry, E. A., Huang, L. S., Saechao, L. K., Pon, N. G., Valkova-Valchanova, M., and Daldal, F. (2004) X-ray Structure of *Rhodobacter capsulatus* Cytochrome bc (1): Comparison with its Mitochondrial and Chloroplast Counterparts, *Photosynth. Res. 81*, 251−75.
8. Stahlberg, H., Dubochet, J., Vogel, H., and Ghosh, R. (1998) The reaction centre of the photounit of *Rhodospirillum rubrum* is anchored to the light-harvesting complex with 4-fold rotational disorder, *Photosynth. Res. 55*, 363−8.
9. Jamieson, S. J., Wang, P., Qian, P., Kirkland, J. Y., Conroy, M. J., Hunter, C. N., and Bullough, P. A. (2002) Projection structure of the photosynthetic reaction centre-antenna complex of *Rhodospirillum rubrum* at 8.5 Å resolution, *EMBO J. 21*, 3927−35.
10. Scheuring, S., Seguin, J., Marco, S., Levy, D., Robert, B., and Rigaud, J. L. (2003) Nanodissection and high-resolution imaging of the *Rhodopseudomonas viridis* photosynthetic core complex in native membranes by AFM. Atomic force microscopy, *Proc. Natl. Acad. Sci. U.S.A. 100*, 1690−3.
11. Scheuring, S., Sturgis, J., Prima, V., Bernadac, A., Levy, D., and Rigaud, J. (2004) Watching the photosynthetic apparatus in native membranes, *Proc. Natl. Acad. Sci. U.S.A. 101*, 11293−7.
12. Goncalves, R. P., Bernadac, A., Sturgis, J. N., and Scheuring, S. (2005) Architecture of the native photosynthetic apparatus of *Phaeospirillum molischianum*, *J. Struct. Biol. 152*, 221−8.
13. Roszak, A. W., Howard, T. D., Southall, J., Gardiner, A. T., Law, C. J., Isaacs, N. W., and Cogdell, R. J. (2003) Crystal structure of the RC-LH1 core complex from *Rhodopseudomonas palustris*, *Science 302*, 1969−72.
14. Scheuring, S., Goncalves, R. P., Prima, V., and Sturgis, J. N. (2006) The Photosynthetic Apparatus of *Rhodopseudomonas palustris*: Structures and Organization, *J. Mol. Biol. 358*, 83−96.
15. Jungas, C., Ranck, J. L., Rigaud, J. L., Joliot, P., and Vermeglio, A. (1999) Supramolecular organization of the photosynthetic apparatus of *Rhodobacter sphaeroides*, *EMBO J. 18*, 534−42.
16. Siebert, C. A., Qian, P., Fotiadis, D., Engel, A., Hunter, C. N., and Bullough, P. A. (2004) Molecular architecture of photosynthetic membranes in *Rhodobacter sphaeroides*: The role of PufX, *EMBO J. 23*, 690−700.
17. Scheuring, S., Francia, F., Busselez, J., Melandri, B. A., Rigaud, J. L., and Levy, D. (2004) Structural role of PufX in the dimerization of the photosynthetic core complex of *Rhodobacter sphaeroides*, *J. Biol. Chem. 279*, 3620−6.
18. Qian, P., Hunter, C. N., and Bullough, P. A. (2005) The 8.5 Å projection structure of the core RC−LH1−PufX dimer of *Rhodobacter sphaeroides*, *J. Mol. Biol. 349*, 948−60.
19. Scheuring, S., Busselez, J., and Levy, D. (2005) Structure of the dimeric PufX-containing core complex of *Rhodobacter blasticus* by in situ atomic force microscopy, *J. Biol. Chem. 280*, 1426−31.
20. Abresch, E. C., Axelrod, H. L., Beatty, J. T., Johnson, J. A., Nechushtai, R., and Paddock, M. L. (2005) Characterization of a highly purified, fully active, crystallizable RC−LH1−PufX core complex from *Rhodobacter sphaeroides*, *Photosynth. Res. 86*, 61−70.
21. Francia, F., Wang, J., Venturoli, G., Melandri, B. A., Barz, W. P., and Oesterhelt, D. (1999) The reaction center-LH1 antenna complex of *Rhodobacter sphaeroides* contains one PufX molecule which is involved in dimerization of this complex, *Biochemistry 38*, 6834−45.
22. Francia, F., Wang, J., Zischka, H., Venturoli, G., and Oesterhelt, D. (2002) Role of the N- and C-terminal regions of the PufX protein in the structural organization of the photosynthetic core complex of *Rhodobacter sphaeroides*, *Eur. J. Biochem. 269*, 1877−85.
23. Comayras, F., Jungas, C., and Lavergne, J. (2005) Functional consequences of the organization of the photosynthetic apparatus in *Rhodobacter sphaeroides*. I. Quinone domains and excitation transfer in chromatophores and reaction center·antenna complexes, *J. Biol. Chem. 280*, 11203−13.
24. Comayras, F., Jungas, C., and Lavergne, J. (2005) Functional consequences of the organization of the photosynthetic apparatus in *Rhodobacter sphaeroides*: II. A study of PufX membranes, *J. Biol. Chem. 280*, 11214−23.
25. Georgakopoulou, S., van der Zwan, G., Olsen, J. D., Hunter, C. N., Niederman, R. A., and van Grondelle, R. (2006) Investigation of the effects of different carotenoids on the absorption and CD signals of light harvesting 1 complexes, *J. Phys. Chem. B 110*, 3354−61.
26. Barz, W. P., Francia, F., Venturoli, G., Melandri, B. A., Vermeglio, A., and Oesterhelt, D. (1995) Role of PufX protein in photosynthetic growth of *Rhodobacter sphaeroides*. 1. PufX is required for efficient light-driven electron transfer and photophosphorylation under anaerobic conditions, *Biochemistry 34*, 15235−47.
27. Frese, R. N., Olsen, J. D., Branvall, R., Westerhuis, W. H., Hunter, C. N., and van Grondelle, R. (2000) The long-range supraorganization of the bacterial photosynthetic unit: A key role for PufX, *Proc. Natl. Acad. Sci. U.S.A. 97*, 5197−202.
28. Frese, R., Siebert, C., Niederman, R., Hunter, C., Otto, C., and van Grondelle, R. (2004) The long-range organization of a native photosynthetic membrane, *Proc. Natl. Acad. Sci. U.S.A. 101*, 17994−9.
29. Bahatyrova, S., Frese, R. N., Siebert, C. A., Olsen, J. D., Van Der Werf, K. O., Van Grondelle, R., Niederman, R. A., Bullough, P. A., Otto, C., and Hunter, C. N. (2004) The native architecture of a photosynthetic membrane, *Nature 430*, 1058−62.
30. Tsukatani, Y., Matsuura, K., Masuda, S., Shimada, K., Hiraishi, A., and Nagashima, K. V. P. (2004) Phylogenetic distribution of unusual triheme to tetraheme cytochrome subunit in the reaction center complex of purple photosynthetic bacteria, *Photosynth. Res. 79*, 83−91.
31. Hiraishi, A., and Hoshino, Y. (1984) Distribution of rhodoquinone in Rhodospirillaceae and its taxonomic implications, *J. Gen. Appl. Microbiol. 30*, 435−48.
32. Barz, W. P., and Oesterhelt, D. (1994) Photosynthetic deficiency of a pufX deletion mutant of *Rhodobacter sphaeroides* is suppressed by point mutations in the light-harvesting complex genes pufB or pufA, *Biochemistry 33*, 9741−52.
33. Francia, F., Dezi, M., Rebecchi, A., Mallardi, A., Palazzo, G., Melandri, B. A., and Venturoli, G. (2004) Light-harvesting complex 1 stabilizes P^+QB^- charge separation in reaction centers of *Rhodobacter sphaeroides*, *Biochemistry 43*, 14199−210.
34. Venturoli, G., Fernandez-Velasco, J. G., Crofts, A. R., and Melandri, B. A. (1986) Demonstration of a collisional interaction of ubiquinol with the ubiquinol-cytochrome c_2 oxidoreductase complex in chromatophores from *Rhodobacter sphaeroides*, *Biochim. Biophys. Acta 851*, 340−52.
35. Cheng, Y., Wolf, E., Larvie, M., Zak, O., Aisen, P., Grigorieff, N., Harrison, S. C., and Walz, T. (2006) Single particle reconstructions of the transferrin-transferrin receptor complex obtained with different specimen preparation techniques, *J. Mol. Biol. 355*, 1048−65.
36. Pascual-Montano, A., Donate, L., Valle, M., Barcena, M., Pascual-Marqui, R., and Carazo, J. M. (2001) A novel neural network technique for analysis and classification of EM single-particle images, *J. Struct. Biol. 133*, 233−45.
37. Scheres, S. H., Valle, M., Nunez, R., Sorzano, C. O., Marabini, R., Herman, G. T., and Carazo, J. M. (2005) Maximum-likelihood multi-reference refinement for electron microscopy images, *J. Mol. Biol. 348*, 139−49.
38. Marco, S., Chagoyen, M., Fraga, L. G., Carazo, J. M., and Carrascosa, J. L. (1996) A variant to the random approximation of the reference-free alignment algorithm, *Ultramicroscopy 66*, 510−5.
39. Sorzano, C. O., Marabini, R., Velazquez-Muriel, J., Bilbao-Castro, J. R., Scheres, S. H., Carazo, J. M., and Pascual-Montano, A. (2004) XMIPP: A new generation of an open-source image processing package for electron microscopy, *J. Struct. Biol. 148*, 194−204.

40. Frank, J., Radermacher, M., Penczek, P., Zhu, J., Li, Y., Ladjadj, M., and Leith, A. (1996) SPIDER and WEB: Processing and visualization of images in 3D electron microscopy and related fields, *J. Struct. Biol. 116*, 190−9.
41. Dutton, P. L., and Jackson, J. B. (1972) Thermodynamic and kinetic characterization of electron-transfer components in situ in *Rhodopseudomonas spheroides* and *Rhodospirillum rubrum*, *Eur. J. Biochem. 30*, 495−510.
42. Moss, D., Leonhard, M., Bauscher, M., and Mantele, W. (1991) Electrochemical redox titration of cofactors in the reaction center from *Rhodobacter sphaeroides*, *FEBS Lett. 283*, 33−6.
43. Crofts, A. R., and Berry, E. A. (1998) Structure and function of the cytochrome bc_1 complex of mitochondrial and photosynthetic bacteria, *Curr. Opin. Struct. Biol. 8*, 501−9.
44. Barz, W. P., Vermeglio, A., Francia, F., Venturoli, G., Melandri, B. A., and Oesterhelt, D. (1995) Role of the PufX protein in photosynthetic growth of *Rhodobacter sphaeroides*. 2. PufX is required for efficient ubiquinone/ubiquinol exchange between the reaction center QB site and the cytochrome bc_1 complex, *Biochemistry 34*, 15248−58.
45. Scheuring, S., Seguin, J., Marco, S., Levy, D., Breyton, C., Robert, B., and Rigaud, J. L. (2003) AFM characterization of tilt and intrinsic flexibility of *Rhodobacter sphaeroides* light harvesting complex 2 (LH2), *J. Mol. Biol. 325*, 569−80.
46. Scheuring, S., Rigaud, J. L., and Sturgis, J. N. (2004) Variable LH2 stoichiometry and core clustering in native membranes of *Rhodospirillum photometricum*, *EMBO J. 23*, 4127−33.
47. Farchaus, J. W., Barz, W. P., Grunberg, H., and Oesterhelt, D. (1992) Studies on the expression of the pufX polypeptide and its requirement for photoheterotrophic growth in *Rhodobacter sphaeroides*, *EMBO J. 11*, 2779−88.
48. Lilburn, T. G., Haith, C. E., Prince, R. C., and Beatty, J. T. (1992) Pleiotropic effects of pufX gene deletion on the structure and function of the photosynthetic apparatus of *Rhodobacter capsulatus*, *Biochim. Biophys. Acta 1100*, 160−70.
49. Parkes-Loach, P. S., Law, C. J., Recchia, P. A., Kehoe, J., Nehrlich, S., Chen, J., and Loach, P. A. (2001) Role of the core region of the PufX protein in inhibition of reconstitution of the core light-harvesting complexes of *Rhodobacter sphaeroides* and *Rhodobacter capsulatus*, *Biochemistry 40*, 5593−601.
50. Aklujkar, M., and Beatty, J. T. (2006) Investigation of *Rhodobacter capsulatus* PufX interactions in the core complex of the photosynthetic apparatus, *Photosynth. Res.* (in press).
51. Hucke, O., Schiltz, E., Drews, G., and Labahn, A. (2003) Sequence analysis reveals new membrane anchor of reaction centre-bound cytochromes possibly related to PufX, *FEBS Lett. 535*, 166−70.

BI0610000